

# Local Atomic Strain in $\text{ZnSe}_{1-x}\text{Te}_x$ from High Real Space Resolution Neutron Pair Distribution Function Measurements

P. F. Peterson, Th. Proffen, I.-K. Jeong, S. J. L. Billinge  
*Department of Physics and Astronomy and Center for Fundamental Materials Research,  
Michigan State University, East Lansing, Michigan 48824-1116, USA*

K.-S. Choi, M. G. Kanatzidis  
*Department of Chemistry, Michigan State University  
East Lansing, Michigan 48824-1116, USA*

P. G. Radaelli  
*ISIS, Rutherford Appleton Laboratory  
Chilton, Didcot OX11 0QX, UK  
(September 22, 2000)*

High real-space resolution atomic pair distribution functions (PDFs) have been obtained from  $\text{ZnSe}_{1-x}\text{Te}_x$  using neutron powder diffraction. Distinct Zn-Se and Zn-Te nearest neighbor (nn) bonds, differing in length by  $\Delta r = 0.14 \text{ \AA}$ , are resolved in the measured PDF allowing the evolution with composition of the individual bond-lengths to be studied. The local bond-lengths change much more slowly with doping than the average bond-length obtained crystallographically. The nn bond-length distributions are constant with doping but higher-neighbor pair distributions broaden significantly indicating that most of the strain from the alloying is accommodated by bond-bending forces in the alloy. The PDFs of alloys across the whole doping range are well fit using a model based on the Kirkwood potential. The resulting PDFs give excellent agreement with the measured PDFs over the entire alloy range with no adjustable parameters.

61.12.-q,61.12.Ld,61.43.-j,61.66.Dk,61.82.Fk,81.05.Dz

## I. INTRODUCTION

Ternary alloys, such as  $\text{ZnSe}_{1-x}\text{Te}_x$ , are technologically useful because the band-gap can be tuned between the end-member values as the composition,  $x$ , is varied. This makes the proper characterization of these materials the subject of much investigation.<sup>1-4</sup>  $\text{ZnSe}_{1-x}\text{Te}_x$  is an example of a II-VI semiconductor pseudobinary alloy that can be made over the entire range of compositions.<sup>5</sup> II-VI alloys are becoming increasingly important because they are often used as the basis for magnetic semiconductors with the additional alloying of small amounts of Mn on the metal sublattice.<sup>6,7</sup> The recent suggestion that high-speed logical circuits can be made out of devices using spin diffusion instead of electron diffusion (so-called “spintronics”) is adding extra impetus to research into these materials.<sup>8</sup> Clearly, it is important to be able to characterize the structure and electronic structure of these alloys in detail.

The study of alloys is complicated by the fact that considerable local atomic strains are present due to the disordering effect of the alloying. This means that local bond-lengths can differ from those inferred from the average (crystallographic) structure by as much as  $0.1 \text{ \AA}$ .<sup>9,10</sup> This clearly has a significant effect on calculations of electronic and transport properties.<sup>2</sup> To fully characterize the structure of these alloys it is necessary to augment crystallography with local structural measurements. In the past the extended x-ray absorption fine structure (XAFS) technique has been extensively used.<sup>9,11,12</sup> More recently the atomic pair distribution function (PDF) analysis of

powder diffraction data has also been applied to get additional local structural information from  $\text{In}_x\text{Ga}_{1-x}\text{As}$  alloys.<sup>10,13,14</sup> In that case high energy x-rays combined with good resolution and a wide range of momentum transfer allow the In-As and Ga-As nearest neighbor peaks to be resolved. In this paper we describe PDF measurements of the II-VI alloy  $\text{ZnSe}_{1-x}\text{Te}_x$  from neutron powder diffraction measurements using the new General Materials Diffractometer (GEM) at ISIS. In these measurements the distinct Zn-Se and Zn-Te bonds, which differ in length by just  $\Delta r = 0.14 \text{ \AA}$ , could be distinguished demonstrating the quality of the data from GEM.

Both ZnTe and ZnSe have the zinc-blende structure ( $F\bar{4}3m$ ) where the Zn atoms and Te, Se atoms occupy the two interpenetrating face-centered-cubic (fcc) lattices. In the alloys the lattice parameter of  $\text{ZnSe}_{1-x}\text{Te}_x$  interpolates linearly between the end member values consistent with Vegard’s law.<sup>15</sup> However, both XAFS experiments<sup>11,12</sup> and theory<sup>16-19</sup> show that the atomic nearest neighbor (nn) distances deviate strongly from Vegard’s law. Rather, they stay closer to their natural lengths found in the end-member compounds:  $L_{\text{Zn-Te}}^0 = 2.643(2) \text{ \AA}$  and  $L_{\text{Zn-Se}}^0 = 2.452(2) \text{ \AA}$ .

A limitation of the XAFS method for studying the local structure of alloys is that it only gives information about the first and second neighbor bond-lengths and information about the bond-length distributions with less accuracy. In this study the PDF analysis of neutron powder diffraction data is used. The PDF is the instantaneous atomic number density-density correlation function which describes the atomic arrangement of the materials. It is the Sine Fourier transform of the exper-

imentally observed total scattering structure function,  $S(Q)$ , obtained from a powder diffraction experiment. Since the total scattering structure function includes both the Bragg and diffuse scattering, the PDF contains both *local* and *average* atomic structure yielding accurate information on short and intermediate length-scales. Previous high resolution PDF studies on  $\text{In}_x\text{Ga}_{1-x}\text{As}$  were carried out using high energy x-ray diffraction.<sup>10,14</sup> This yielded data over a wide  $Q$ -range ( $Q$  is the magnitude of the scattering vector) which resulted in the very high real-space resolution required to separate the nearest neighbor peaks from In-As and Ga-As. The high  $Q$ -range coverage and  $Q$ -space resolution of the new General Materials (GEM) Diffractometer at the ISIS neutron source allowed us, for the first time, to obtain similarly high real space resolution PDFs of  $\text{ZnSe}_{1-x}\text{Te}_x$  using neutrons and to resolve the Zn-Se and Zn-Te bonds that differ in length by only 0.14 Å. Furthermore, the data collection time was only sixty minutes compared to the 12 hours for the x-ray data with similar quality. The nn distances and average peak widths are fit using model independent techniques. The PDFs of the full alloy series have been calculated using a model based on the Kirkwood potential giving excellent agreement over a wide range of  $r$  with no adjustable parameters.

## II. EXPERIMENTAL

### A. Synthesis and Characterization

Finely powdered samples of  $\sim 10\text{g}$  of  $\text{ZnSe}_{1-x}\text{Te}_x$  were made with  $x = \frac{1}{6}, \frac{2}{6}, \frac{3}{6}, \frac{4}{6}, \frac{5}{6}$ . The starting reagents (zinc selenide, metal basis, 99.995%; zinc telluride, metal basis, 99.999%) were finely ground, mixed in the correct stoichiometry, and sealed in quartz tubes under vacuum. The samples were then heated at  $900^\circ\text{C}$  for 12-16 hours.<sup>20</sup> This procedure (grinding, vacuum sealing, and heating) was repeated four times to obtain high quality homogeneous products. The colors of the solid solutions vary gradually from dark red (ZnTe) to yellow (ZnSe) as the  $x$ -value decreases reflecting the band-gap of the alloy samples smoothly changing in the optical frequency range. The homogeneity of the samples was checked using x-ray diffraction by monitoring the width and line-shape of the  $\langle 400 \rangle$ ,  $\langle 331 \rangle$ ,  $\langle 420 \rangle$ , and  $\langle 422 \rangle$  Bragg peaks measured on a rotating anode Cu  $K_\alpha$  source. Finely powdered samples were sieved through a 200-mesh sieve then packed into flat plates and measured in symmetric reflection geometry. The  $\langle 331 \rangle$  and (weak on high angle side)  $\langle 420 \rangle$  peaks are reproduced in Fig. 1. The double-peaked shape comes from the  $K_{\alpha 1}$  and  $K_{\alpha 2}$  components in the beam. The line-widths are narrow and smoothly interpolate in position between the positions of the end-members verifying the homogeneity of the samples.

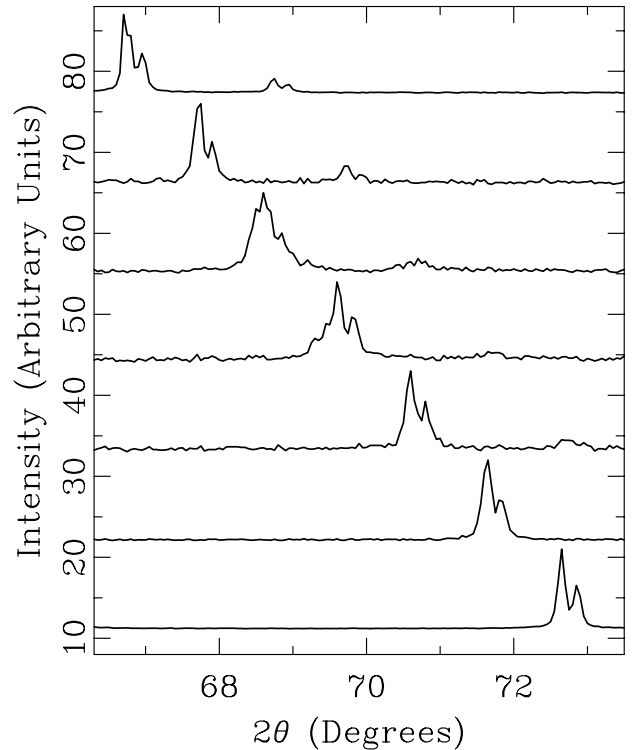


FIG. 1.  $\langle 331 \rangle$  and weak  $\langle 420 \rangle$  peaks of  $\text{ZnSe}_{1-x}\text{Te}_x$  at (from top to bottom)  $x = 1, \frac{5}{6}, \frac{4}{6}, \frac{3}{6}, \frac{2}{6}, \frac{1}{6}, 0$  measured at 300K using Cu rotating anode.

### B. Neutron Measurements and Data Processing

Time of flight neutron powder diffraction data were measured on the GEM diffractometer at the ISIS spallation neutron source at Rutherford Appleton Laboratory in Oxfordshire, UK. The finely powdered  $\text{ZnSe}_{1-x}\text{Te}_x$  samples were sealed inside extruded cylindrical vanadium containers. These were mounted on the cold-stage of a helium cryostat immersed in cold He gas in contact with a liquid He reservoir. The temperature of the samples was maintained at 10K using a heater attached to the cold-stage adjacent to the sample. The empty cryostat, an empty container mounted on the cryostat and the empty instrument were all measured, allowing us to assess and subtract instrumental backgrounds. The scattering from a vanadium rod was also measured to allow the data to be normalized for the incident spectrum and detector efficiencies. Standard data corrections were carried out as described elsewhere<sup>21,22</sup> using the program PDFgetN.<sup>23</sup> After being corrected the data are normalized by the total scattering cross-section of the sample to yield the total scattering structure function,  $S(Q)$ . This is then converted to the PDF,  $G(r)$ , by a Sine Fourier transform according to

$$G(r) = \frac{2}{\pi} \int_0^\infty Q[S(Q) - 1] \sin(Qr) dQ = 4\pi r(\rho(r) - \rho_0), \quad (1)$$

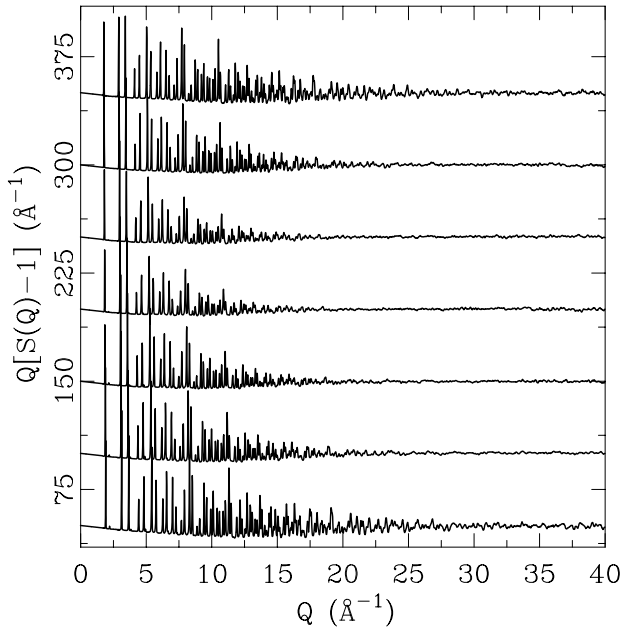


FIG. 2.  $Q[S(Q) - 1]$  for  $\text{ZnSe}_{1-x}\text{Te}_x$  at (from top to bottom)  $x = 1, \frac{5}{6}, \frac{4}{6}, \frac{3}{6}, \frac{2}{6}, \frac{1}{6}, 0$  measured at 10K.

where  $\rho(r)$  is the microscopic pair density of the sample and  $\rho_0$  is the average number density.

The GEM instrument yields useful diffraction information up to a maximum  $Q$  of greater than  $90 \text{ \AA}^{-1}$ . Unfortunately, due to a neutron resonance in Te we were forced to terminate the Fourier transform at a maximum  $Q$  of  $40 \text{ \AA}^{-1}$  in this experiment. This resulted in nn peaks in these alloys which are resolution limited rather than sample limited. This was verified by Fourier transforming the ZnSe end-member at higher values of  $Q_{max}$ . The nn peak kept getting sharper up to  $Q_{max} = 60 \text{ \AA}^{-1}$ . Nonetheless, the distinct short and long bond distances are still evident in the alloy PDFs. At the time of this measurement the backscattering detector banks on GEM were not operational. With the backscattering banks yielding better statistics in high  $Q$  and adding detector coverage, one might expect to get similar quality PDFs in a fraction of the time. The reduced structure functions,  $Q[S(Q) - 1]$ , obtained from the  $\text{ZnSe}_{1-x}\text{Te}_x$  samples are shown in Fig. 2 and the resulting PDFs are shown in Fig. 3.

### C. Method of Modeling

The PDF can be calculated from a structural model by taking advantage of the definition of radial distribution function (RDF),<sup>21</sup>  $T(r)$ ,

$$T(r) = 4\pi r^2 \rho(r) = \sum_{i,j} \frac{b_i b_j}{\langle b \rangle^2} \delta(r - r_{ij}), \quad (2)$$

and substituting the calculated  $\rho(r)$  into Eq. 1. Here  $b_i$  is the scattering length of the  $i$ th atom,  $\langle b \rangle$  is the scattering

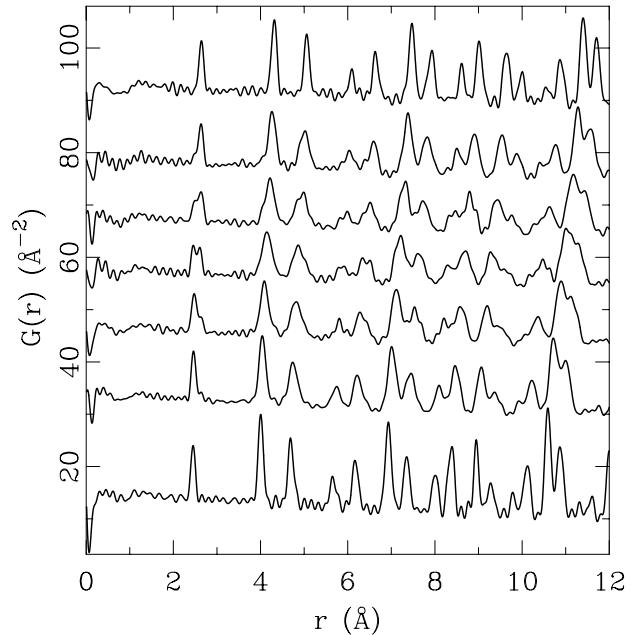


FIG. 3.  $G(r) = 4\pi r(\rho(r) - \rho_0)$  for  $\text{ZnSe}_{1-x}\text{Te}_x$  at (from top to bottom)  $x = 1, \frac{5}{6}, \frac{4}{6}, \frac{3}{6}, \frac{2}{6}, \frac{1}{6}, 0$  measured at 10K.

length averaged over the sample composition and isotopes,  $r_{ij} = |\mathbf{r}_i - \mathbf{r}_j|$  is the distance separating the  $i$ th and  $j$ th atoms and the sums are taken over all the atoms in the entire sample. To approximate the atomic thermal motion we convolute the delta-functions with Gaussians. Before being compared to the data the calculated  $G(r)$  is convoluted with a termination function,  $\sin(Q_{max}r)/r$ , to account for the effects of the finite range of the measured data.<sup>24,25</sup>

We have used three approaches to obtain structural information from the PDF. First, we carry out a model independent analysis by fitting Gaussian functions to peaks in the RDF. Next we calculate the PDF expected from the average crystal structure and refine, using a least squares approach, atomic displacement (thermal) parameters to obtain empirically the PDF peak widths in the alloys. This is done using the PDF refinement program PDFFIT.<sup>26</sup> Finally, we calculate the PDF from a Kirkwood potential based model where the atom positions and thermal broadenings are fully determined by the atomic potential parameters.

The ZnSe and ZnTe nn distances in the alloys were found by fitting two Gaussians, convoluted with termination functions to account for the termination effects, to the nearest neighbor peak in the PDF. Peak positions and widths were varied. The relative peak intensities were constrained to those expected from the alloy composition. The widths refined to the same values as the end-members within the errors for all the alloys. We thus repeated the fits constraining the peak widths to have the values refined from the end-member PDFs. This more highly constrained fitting procedure resulted in less scatter in the refined peak positions.

To find the far neighbor peak widths PDFFIT<sup>26</sup> was used.

TABLE I.  $\alpha$  and  $\beta$  reported for  $\text{ZnSe}_{1-x}\text{Te}_x$  and  $\text{In}_x\text{Ga}_{1-x}\text{As}$ .<sup>17</sup>

	$\alpha$ (N/m)	$\beta$ (N/m)	$\beta/\alpha$	$a^{**}$
ZnSe	33.7	4.6	0.14	0.78
ZnTe	31.1	4.7	0.15	0.76
InAs	35.1	5.8	0.16	0.74
GaAs	44.3	9.2	0.21	0.70

The zinc-blende crystal structure was used with all the atoms constrained to lie on their average positions. Lattice parameters, scale factor, isotropic thermal factors, and  $r$ -dependent PDF peak broadening parameters<sup>24,26</sup> were allowed to vary but the atoms were not allowed to move off their sites. In this way, all of the atomic disorder, static and dynamic, is included in the refined thermal factors that are giving an empirical measure of the PDF peak widths at higher- $r$ . This approach is better than fitting unconstrained Gaussians because of the problem of PDF peak overlap at higher distances. Clearly this approach does not result in a good model for the alloy structure but will yield a good fit to the intermediate PDF in the alloys. However, it should give reliable empirical estimates of the width of high- $r$  PDF peaks, even when they are strongly overlapped, and allows us to separate the disorder on the cation and anion sublattices. The PDFs were fit over the range of 3 to 15  $\text{\AA}^{-1}$ . This range was selected so the global properties of the alloys could be fit without influence from the nn behavior.

Potential based modeling to yield realistic alloy structures has been carried out using a model based on the Kirkwood potential.<sup>27</sup> This procedure has been described in detail elsewhere.<sup>16,17,28,29</sup> The model consists of 512 atoms arranged in the zinc-blende structure with periodic boundary conditions where the interatomic force is described by the Kirkwood potential. The system is then relaxed by moving atoms to minimize the energy.

The Kirkwood potential can be written as,

$$V = \frac{\alpha}{2} \sum_{ij} (L_{ij} - L_{ij}^0)^2 + \frac{\beta}{8} \sum_{ijk} (\cos \theta_{ijk} + \frac{1}{3})^2, \quad (3)$$

where  $L_{ij}$  is the length of the bond between the atoms  $i$  and  $j$  and  $L_{ij}^0$  is the natural bond-length. In this definition the bond-stretching,  $\alpha$ , and bond-bending,  $\beta$ , force constants have the same units and  $\theta_{ijk} = \arccos(-\frac{1}{3})$ , for an ideal tetrahedron. Literature values<sup>30</sup> were used for the bond-stretching and bond-bending parameters obtained from elastic constant measurements. We also tried optimizing  $\alpha$  and  $\beta$  by fitting to the ZnSe and ZnTe end-member PDFs; however, the PDFs calculated using both sets of parameters gave comparable agreement when compared to the alloy data so we simply report the results obtained with the literature values of  $\alpha$  and  $\beta$ . The values of  $\alpha$  and  $\beta$  for ZnTe and ZnSe used are shown in Table I.

The PDFs for the alloys are calculated with no adjustable parameters using the same potential parameters used for the end-members. The additional bond-bending parameters present in the alloy due to Te-Zn-Se type configurations are determined as a geometric mean of the  $\beta$  parameters for the

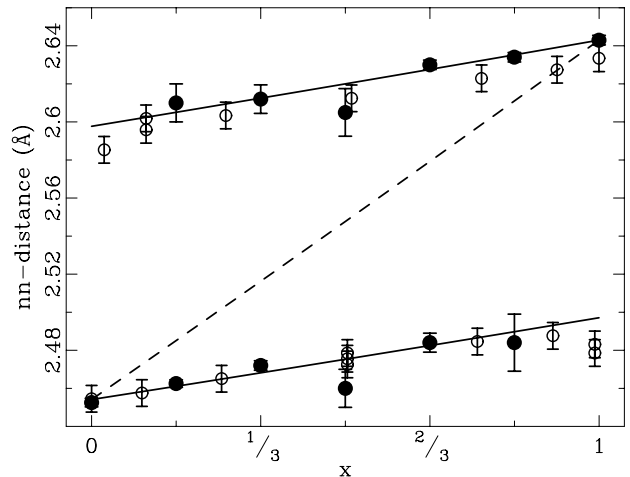


FIG. 4. nn positions from the PDF ( $\bullet$ ), XAFS data<sup>12</sup> ( $\circ$ ), and Kirkwood model z-plot (solid line)<sup>17</sup> as a function of composition,  $x$ , for  $\text{ZnSe}_{1-x}\text{Te}_x$ . The dashed line is the average nn distance. Note that not all XAFS points had reported error bars so they were all set to the same value.

end-members.<sup>28</sup> The thermal broadening of the PDF is calculated by determining the dynamical matrix from the potential and projecting out the atomic displacement amplitudes for each phonon.<sup>28</sup>

### III. RESULTS AND DISCUSSION

#### A. Model Independent Results

Upon inspection of the PDFs presented in Fig. 3 one will immediately notice the splitting of the first peak. This comes from the fact that the nn distances of ZnTe and ZnSe stay close to the end-member values of 2.643(2) $\text{\AA}$  and 2.452(2) $\text{\AA}$  respectively. The positions of each component of the doublet were determined by fitting Gaussians as described above. The values for the nn bond-lengths are shown as filled circles with  $2\sigma$  error bars in Fig. 4. Also plotted in the same Figure are the nn bond-lengths determined from an earlier XAFS study by Boyce and Mikkelsen.<sup>12</sup> There is clearly excellent agreement between the two results. Superimposed on the data are lines which are the predictions of the Kirkwood model for the nearest neighbor bond-lengths using the potential parameters given in Table I.<sup>17</sup> Again, there is excellent agreement with the data with no adjustable parameters.

In contrast to the local structure, the long-range structure is well described by the virtual crystal approximation (VCA).<sup>31,32</sup> The VCA assumes that the structural properties of a crystal alloy all are a linear interpolation of the end-member values. If this were true in semiconductor alloys then not only would one be able to find the lattice parameter of the alloy from Vegard's law but the nn distance would be, for zinc-blende crystals  $\text{A}_{1-x}\text{B}_x\text{C}$ ,  $L_{AC} = L_{BC} = \frac{\sqrt{3}}{4}a$ . This is shown in Fig. 4 as the dashed line.

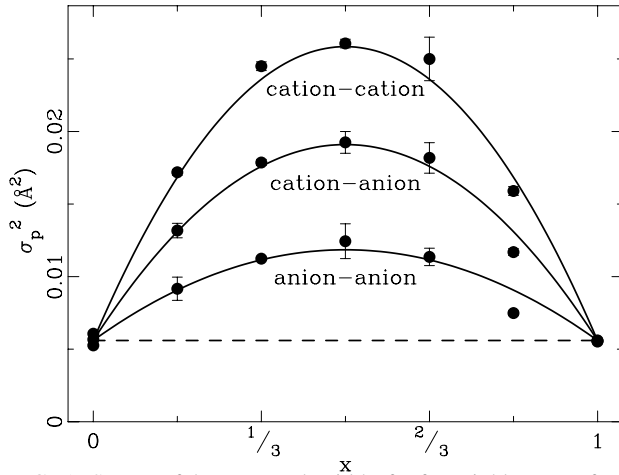


FIG. 5. Square of the PDF peak widths for far neighbors as a function of composition,  $x$ . The extracted values (points) are plotted with parabolas (lines) to guide the eye. The dotted line is at  $0.0056\text{\AA}^2$ .

It is clear that the local bond-lengths remain closer to those in the end-members than to the prediction of Vegard's law. In fact the bond-lengths stay close to the Pauling limit<sup>33</sup> in which they would remain completely unchanged in length across the alloy series. The deviation from the Pauling limit is attributed to the disorder in the force constants as we describe below.

The difference in the local structure of the alloys leads to a large amount of atomic strain resulting in much broader PDF peaks in the high- $r$  region of the PDF. In Fig. 5 the strain is quantified. The dotted line at  $\sigma_p^2 = 0.0056\text{\AA}^2$  represents the mean square width of the PDF peak,  $\sigma_p^2$ , attributed to the thermal motion of the atoms while the parabolas indicate additional peak broadening due entirely to static strain in the system. The largest peak broadening is seen in the mean-square width of the Zn-Zn peaks (cation-cation) which is as much as  $5\times$  as large as the mean-square width due to thermal broadening and zero-point motion at 10 K. It is also evident that the disorder is larger on the unalloyed (Zn) sublattice than the mixed (Se,Te) sublattice similar to the observation in  $\text{In}_x\text{Ga}_{1-x}\text{As}$ .<sup>10,14</sup>

### B. Kirkwood Model

The Kirkwood potential<sup>27</sup> is widely used to describe semiconductor alloys. Petkov *et al.*<sup>10</sup> showed that the Kirkwood model is good at describing  $\text{In}_x\text{Ga}_{1-x}\text{As}$ , a III-V semiconductor.  $\text{ZnSe}_{1-x}\text{Te}_x$  is a II-VI semiconductor so it is of great interest to know whether or not the Kirkwood model is equally successful for this more polar semiconductor alloy. The values of  $\alpha$  and  $\beta$  used in this study are shown in Table I with with appropriate values for  $\text{In}_x\text{Ga}_{1-x}\text{As}$  for comparison.

Other quantities of note are the ratio,  $\beta/\alpha$ , and the topological rigidity parameter,  $a^{**}$ ,<sup>16</sup> which is a function of  $\beta/\alpha$ :

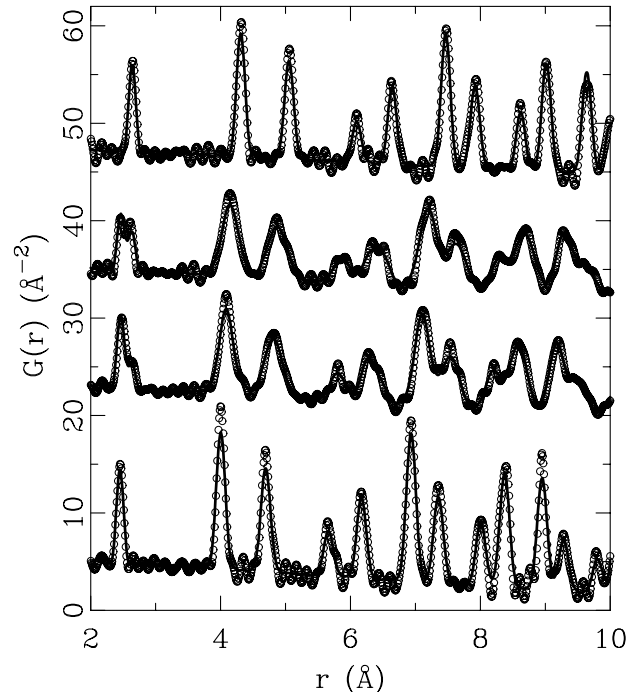


FIG. 6. Comparison of the Kirkwood model (lines) and data ( $\circ$ ) PDFs for (from top to bottom) ZnTe,  $\text{ZnSe}_{3/6}\text{Te}_{3/6}$ ,  $\text{ZnSe}_{4/6}\text{Te}_{2/6}$ , and ZnSe.

$$a^{**} = \frac{1 + 1.25(\beta/\alpha)}{1 + 3.6(\beta/\alpha) + 1.17(\beta/\alpha)^2}. \quad (4)$$

The topological rigidity parameter,  $a^{**}$ , can vary from 0 to 1 and quantifies the effect of the lattice. The Pauling limit results when  $a^{**}=0$ , the floppy lattice limit. If  $a^{**}=1$  the lattice is rigid and Vegard's law will hold true locally as well as globally. As can be seen in Table I, the values found for  $a^{**}$  are close to 0.75 which appears to be fairly universal for all semiconductors.<sup>16</sup>

In this study, the  $z$ -plot shown in Fig. 4 and PDFs from each alloy composition were all calculated using the Kirkwood parameters appropriate for the end-members with no adjustable parameters. Fig. 6 shows PDFs obtained from the Kirkwood model plotted with measured PDFs for characteristic compositions. The model is very successful in matching both the short *and* longer-range behavior of the PDFs for all alloy compositions. The measured and calculated PDF peaks of the nearest neighbor bonds are shown on an expanded scale in Fig. 7. It is clear that the model based on the Kirkwood potential does a very satisfactory job of explaining both the PDF peak positions and widths and appears to produce a very satisfactory model for the structure of these II-VI alloys.

### C. Comparison with $\text{In}_x\text{Ga}_{1-x}\text{As}$

The results found for  $\text{ZnSe}_{1-x}\text{Te}_x$  are not entirely unexpected. In a previous study of  $\text{In}_x\text{Ga}_{1-x}\text{As}$  similar results

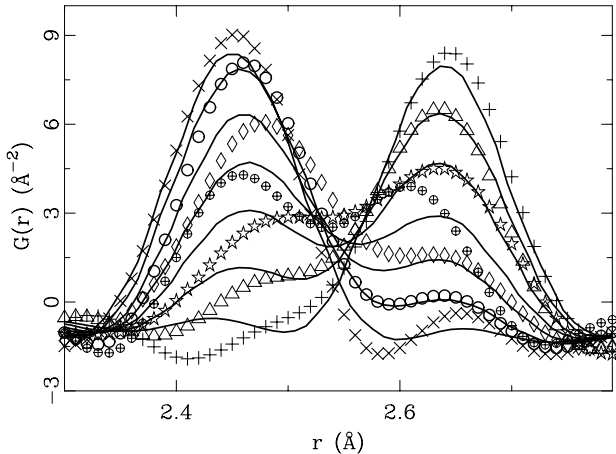


FIG. 7. Comparison of the Kirkwood model (lines) and data (points) nn distances for  $\text{ZnSe}_{1-x}\text{Te}_x$  where  $x$  is 0 ( $\times$ ),  $\frac{1}{6}$  ( $\circ$ ),  $\frac{2}{6}$  ( $\diamond$ ),  $\frac{3}{6}$  ( $\oplus$ ),  $\frac{4}{6}$  ( $\star$ ),  $\frac{5}{6}$  ( $\triangle$ ), and 1 ( $+$ ).

TABLE II. Ionic radii from literature when atoms are in tetrahedral covalent bonds.<sup>34</sup>

A - B	$r_A$ (Å)	$r_B$ (Å)	$r_{A+B}$ (Å)
GaAs	1.26	1.18	2.44
InAs	1.44	1.18	2.62
ZnSe	1.31	1.14	2.45
ZnTe	1.31	1.32	2.63

were obtained.<sup>10</sup> With high real space resolution measurements now possible, direct observation of the nn distances in addition to the static strain in the system is observed. The basis for the comparison between  $\text{ZnSe}_{1-x}\text{Te}_x$  and  $\text{In}_x\text{Ga}_{1-x}\text{As}$  is that the two systems are both semiconductor alloys with zinc-blende structures. However, they vary in a couple of important aspects. The salient difference is number of valence electrons.  $\text{ZnSe}_{1-x}\text{Te}_x$  are more polar alloys and so might be expected to have bonding with more ionic character than  $\text{In}_x\text{Ga}_{1-x}\text{As}$  which should give rise to smaller  $\beta$  values since ionic bonding is less directional than covalent bonding. Indeed the bond-bending magnitudes are less in  $\text{ZnSe}_{1-x}\text{Te}_x$  than  $\text{In}_x\text{Ga}_{1-x}\text{As}$  (Tab. I). However, the nearest neighbor bonds are stiffer in  $\text{In}_x\text{Ga}_{1-x}\text{As}$ . This is presumably also due to the lower polarity of this material resulting in greater orbital overlap and covalency. The result is that the  $\beta/\alpha$  ratio and  $a^{**}$  are similar for the two systems. Since it is this ratio, rather than the values of  $\alpha$  and  $\beta$  themselves, that has the greatest impact on the structure of the alloy, we find very strong similarities in the local structures of  $\text{In}_x\text{Ga}_{1-x}\text{As}$  and  $\text{ZnSe}_{1-x}\text{Te}_x$ . For example, the z-plots from both systems are plotted on the same scale in Fig. 8.

The similarity in the z-plots is even more striking because of the similar bond-lengths of the end-members in these two alloy systems. The ionic radii for the atoms in these two alloy series are reproduced in Table II. Despite the ionic radii themselves being somewhat different, it is clear that the sums of the ionic radii of the end-members yield values that are

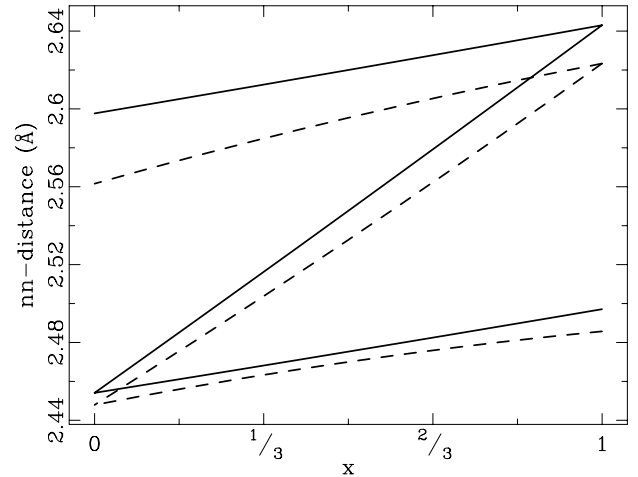


FIG. 8. Comparison of the theoretically calculated  $\text{ZnSe}_{1-x}\text{Te}_x$  (solid line) and  $\text{In}_x\text{Ga}_{1-x}\text{As}$  (dashed line) z-plots.

within 0.01 Å of each other.

As well as the z-plots of  $\text{In}_x\text{Ga}_{1-x}\text{As}$  and  $\text{ZnSe}_{1-x}\text{Te}_x$  matching rather well, the observed magnitude of the mean-square width of the high- $r$  PDFs peak are rather similar in the two alloy series. This can be seen by comparing Fig. 5 with Fig. 4 in Ref. 10. For example, the static strain contribution to the PDF peak widths of the unalloyed site has a maximum at  $0.027\text{Å}^2$  and  $0.023\text{Å}^2$  for  $x = 0.5$  in  $\text{ZnSe}_{1-x}\text{Te}_x$  and  $\text{In}_x\text{Ga}_{1-x}\text{As}$ , respectively.

It thus appears that the structure of the alloys is principally determined by the differences in bond-length of the end-members and by the  $\beta/\alpha$  ratio rather than by the absolute values of  $\alpha$  and  $\beta$  or the absolute values of the ionic radii themselves. It has been shown<sup>16,17</sup> that the  $\beta/\alpha$  ratios of tetrahedral semiconductors are somewhat universal resulting in  $a^{**}$  values close to 0.75 for a wide range of semiconductors. It also does not appear to matter whether the cation or anion sublattice is alloyed. The unalloyed sublattice accommodates the majority of the atomic scale strain.

#### IV. CONCLUSION

From high real space resolution PDFs of  $\text{ZnSe}_{1-x}\text{Te}_x$  we conclude the following. In agreement with earlier XAFS results and the Kirkwood model the Zn-Se and Zn-Te bond-lengths do not take a compositionally averaged length but remain close to their natural lengths. Direct measurement of this was allowed by the new GEM instrument at ISIS. The bond-length mismatch creates considerable local disorder which manifests itself as broadening in the PDF peak widths and can be separated into thermal motion and static strain.  $\text{ZnSe}_{1-x}\text{Te}_x$  was compared with  $\text{In}_x\text{Ga}_{1-x}\text{As}$ . Despite having different polarity the atomic strains in both systems are very similar and both are well modeled by the Kirkwood potential based model. This suggests that the atomic strains in tetrahedral semiconductor alloys are quite universal depending prin-

cipally on the bond-length mismatch of the end-members and the ratio of the bond-stretch to bond-bending forces.

#### ACKNOWLEDGMENTS

The authors thank M. F. Thorpe for making available Kirkwood model programs and for useful discussions concerning the Kirkwood model and to V. Petkov for useful discussions. This work was supported by DOE through Grant No. DE-FG02-97ER45651.

- 
- <sup>1</sup> A. M. Glass, *Science* **235**, 1003 (1985).
  - <sup>2</sup> Z. Q. Li and W. Potz, *Phys. Rev. B* **46**, 2109 (1992).
  - <sup>3</sup> A. Silverman, A. Zunger, R. Kalish, and J. Adler, *Phys. Rev. B* **51**, 10795 (1995).
  - <sup>4</sup> A. Balzarotti, N. Motta, A. Kisiel, M. Zimnal-Starnawska, M. T. Czyżyk, and M. Podgórnny, *Phys. Rev. B* **31**, 7526 (1985).
  - <sup>5</sup> H. Ohtani, K. Kojima, K. Ishida, and T. Nishizawa, *J. Alloy Cmpd.* **182**, 103 (1992).
  - <sup>6</sup> R. Fiederling, M. Kelm, G. Reuscher, W. Ossau, G. Schmidt, A. Wang, and L. Molenkamp, *Nature* **402**, 787 (1999).
  - <sup>7</sup> T. M. Giebultowicz, J. J. Rhyne, W. Y. Ching, D. L. Huber, and J. Furdyna, *J. Appl. Phys.* **63**, 3297 (1988).
  - <sup>8</sup> P. Ball, *Nature* **404**, 918 (2000).
  - <sup>9</sup> J. C. Mikkelsen and J. B. Boyce, *Phys. Rev. Lett.* **49**, 1412 (1982).
  - <sup>10</sup> V. Petkov, I-K. Jeong, J. S. Chung, M. F. Thorpe, S. Kycia, and S. J. L. Billinge, *Phys. Rev. Lett.* **83**, 4089 (1999).
  - <sup>11</sup> J. B. Boyce and J. C. Mikkelsen, Jr., *Phys. Rev. B* **31**, 6903 (1985).
  - <sup>12</sup> J. B. Boyce and J. C. Mikkelsen, Jr., *J. Cryst. Growth* **98**, 37 (1989).
  - <sup>13</sup> V. Petkov, I-K. Jeong, F. Mohiuddin-Jacobs, Th. Proffen, and S. J. L. Billinge, *J. Appl. Phys.* **88**, 665 (2000).
  - <sup>14</sup> I-K. Jeong, F. Mohiuddin-Jacobs, V. Petkov, S. J. L. Billinge, and S. Kycia, *Phys. Rev. B* (2000), submitted.
  - <sup>15</sup> L. Vegard, *Z. Phys.* **5**, 17 (1921).
  - <sup>16</sup> Y. Cai and M. F. Thorpe, *Phys. Rev. B* **46**, 15872 (1992).
  - <sup>17</sup> Y. Cai and M. F. Thorpe, *Phys. Rev. B* **46**, 15879 (1992).
  - <sup>18</sup> N. Mousseau and M. F. Thorpe, *Phys. Rev. B* **46**, 15887 (1992).
  - <sup>19</sup> M. C. Schabel and J. L. Martins, *Phys. Rev. B* **43**, 11,873 (1991).
  - <sup>20</sup> S. Larach, R. E. Shrader, and C. F. Stocker, *Phys. Rev.* **108**, 587 (1957).
  - <sup>21</sup> S. J. L. Billinge and T. Egami, *Phys. Rev. B* **47**, 14386 (1993).
  - <sup>22</sup> C. N. J. Wagner, *J. Non-Crystalline Solids* **31**, 1 (1978).
  - <sup>23</sup> P. F. Peterson, M. Gutmann, Th. Proffen, and S. J. L. Billinge, *J. Appl. Crystallogr.* **33**, 1192 (2000).
  - <sup>24</sup> S. J. L. Billinge, in *Local Structure from Diffraction*, edited by S. J. L. Billinge and M. F. Thorpe, page 137, New York, 1998, Plenum.
  - <sup>25</sup> M. F. Thorpe, J. S. Chung, S. J. L. Billinge, and F. Mohiuddin-Jacobs, in *Local Structure from Diffraction*, edited by S. J. L. Billinge and M. F. Thorpe, page 157, New York, 1998, Plenum.
  - <sup>26</sup> Th. Proffen and S. J. L. Billinge, *J. Appl. Crystallogr.* **32**, 572 (1999).
  - <sup>27</sup> J. G. Kirkwood, *J. Phys. Chem.* **7**, 506 (1939).
  - <sup>28</sup> J. S. Chung and M. F. Thorpe, *Phys. Rev. B* **55**, 1545 (1997).
  - <sup>29</sup> J. S. Chung and M. F. Thorpe, *Phys. Rev. B* **59**, 4807 (1999).
  - <sup>30</sup> Y. Cai and M. F. Thorpe, *Phys. Rev. B* **46**, 15879 (1992).
  - <sup>31</sup> L. Nordheim, *Ann. Phys. (Leipz.)* **9**, 607 (1931).
  - <sup>32</sup> L. Nordheim, *Ann. Phys. (Leipz.)* **9**, 641 (1931).
  - <sup>33</sup> L. Pauling, *The Nature of the Chemical Bond*, Cornell Univ. Press, Ithaca, 1967.
  - <sup>34</sup> C. Kittel, *Introduction to Solid State Physics*, Wiley, New York, 7th edition, 1996.